THE JOURNAL OF BIOLOGICAL CHEMISTRY VOL. 281, NO. 31, pp. 22367–22377, August 4, 2006

Crystal Structure and Mutational Analysis of the DaaE Adhesin of *Escherichia coli*[*]

Received for publication, May 15, 2006 Published, JBC Papers in Press, June 2, 2006, DOI 10.1074/jbc.M604646200

Natalia Korotkova[‡], Isolde Le Trong[§¶], Ram Samudrala[‡], Konstantin Korotkov[‖], Cristina P. Van Loy[‡], Anh-Linh Bui[‡], Steve L. Moseley[‡], and Ronald E. Stenkamp[§¶‖1]

From the [‡]Department of Microbiology, the [§]Department of Biological Structure, [¶]Biomolecular Structure Center, and the [‖]Department of Biochemistry, University of Washington, Seattle, Washington 98195

DaaE is a member of the Dr adhesin family of *Escherichia coli*, members of which are associated with diarrhea and urinary tract infections. A receptor for Dr adhesins is the cell surface protein, decay-accelerating factor (DAF). We have carried out a functional analysis of Dr adhesins, as well as mutagenesis and crystallographic studies of DaaE, to obtain detailed molecular information about interactions of Dr adhesins with their receptors. The crystal structure of DaaE has been solved at 1.48 Å resolution. Trimers of the protein are found in the crystal, as has been the case for other Dr adhesins. Naturally occurring variants and directed mutations in DaaE have been generated and analyzed for their ability to bind DAF. Mapping of the mutation sites onto the DaaE molecular structure shows that several of them contribute to a contiguous surface that is likely the primary DAF-binding site. The DAF-binding properties of purified fimbriae and adhesin proteins from mutants and variants correlated with the ability of bacteria expressing these proteins to bind to human epithelial cells in culture. DaaE, DraE, AfaE-III, and AfaE-V interact with complement control protein (CCP) domains 2–4 of DAF, and analysis of the ionic strength dependence of their binding indicates that the intermolecular interactions are highly electrostatic in nature. The adhesins AfaE-I and NfaE-2 bind to CCP-3 and CCP-4 of DAF, and electrostatic interactions contribute significantly less to these interactions. These observations are consistent with structural predictions for these Dr variants and also suggest a role for the positively charged region linking CCP-2 and CCP-3 of DAF in electrostatic Dr adhesin-DAF interactions.

Bacterial pathogens frequently express adhesins that mediate attachment to the sites of infections. The Dr family of adhesins of *Escherichia coli* is associated with diarrhea and urinary tract infections, in particular cystitis, pyelonephritis, and recurring infections. This family includes Dr hemagglutinin (DraE), Dr-II, DaaE, AfaE-I, AfaE-II, AfaE-III, AfaE-V, and NfaE-111 and others (1). Dr family members such as DraE, DaaE, and Dr-II have been shown to exhibit a fimbrial morphology (2, 3). The fimbrial structure consists largely of a single polymerized subunit. The major structural subunit is also the adhesive subunit (4). Other members of the Dr family are described as afimbrial based on the fact that fimbriae cannot be detected by electron microscopy (5, 6). The fimbriae are assembled via the chaperone/usher pathway, a common assembly mechanism for bacterial appendages (7, 8).

The crystal structures for the type 1 pilus (FimC-FimH), the P pilus (PapD-PapK), and Caf1M-Caf1 complexes (8–10) reveal that the major subunits, including the chaperones, have Ig-like folds. The final β-strand in the fold (strand G) is missing in the structural subunits, creating a deep hydrophobic cleft on the surface. The chaperones insert their β-strand into this cleft to complete the Ig-like fold in a process called donor strand complementation. Assembly of fimbriae proceeds by a donor strand exchange mechanism in which the chaperone β-strand is replaced by a conserved β-strand motif located at the N terminus of a second structural subunit.

Dr adhesins recognize decay-accelerating factor (DAF)[2] as their receptor. DAF is a complement-regulatory protein that protects host tissues from damage by the autologous complement system by inhibiting the formation of C3 and C5 convertases and accelerating their decay (11). DAF is a glycosylphosphatidylinositol-anchored membrane protein present on a variety of epithelial surfaces, including gastrointestinal mucosa, exocrine glands, renal pelvis, ureter, bladder, cervix, and uterine mucosa (12). The extracellular portion of DAF includes four complement control protein domains (CCPs), alternatively known as short consensus repeats (11). The binding of classical pathway (CP) convertases is localized within CCP-2 and CCP-3, whereas regulation of the alternative pathway (AP) extends through to CCP-4 (13). CCP-3 has been identified as the domain involved in binding to the Dr adhesins (14, 15). Activation of complex signal transduction cascades associated with DAF follows the binding of Dr adhesins (1). The attachment of bacteria expressing Dr adhesins to brush border-associated DAF induces clustering of DAF around bacterial cells and also recruitment of the glycosylphosphatidylinositol-anchored brush

[*] This work was supported by NIDDK Grant DK-064229 from the National Institutes of Health. Portions of this research were carried out at the Stanford Synchrotron Radiation Laboratory, a national user facility operated by Stanford University on behalf of the United States Department of Energy, Office of Basic Energy Sciences. The costs of publication of this article were defrayed in part by the payment of page charges. This article must therefore be hereby marked "*advertisement*" in accordance with 18 U.S.C. Section 1734 solely to indicate this fact.

The atomic coordinates and structure factors (code 2BCM) have been deposited in the Protein Data Bank, Research Collaboratory for Structural Bioinformatics, Rutgers University, New Brunswick, NJ (http://www.rcsb.org/).

[1] To whom correspondence should be addressed: Box 357420, Dept. of Biological Structure, University of Washington, Seattle, WA 98195-7420. Tel.: 206-685-1721; Fax: 206-543-1724; E-mail: stenkamp@u.washington.edu.

[2] The abbreviations used are: DAF, decay-accelerating factor; SPR, surface plasmon resonance; CEA, carcinoembryonic antigen; CCP, complement control protein; CP, classical pathway; AP, alternative pathway; CHO, Chinese hamster ovary; CHES, 2-(cyclohexylamino)ethanesulfonic acid; PDB, Protein Data Bank; Cm, chloramphenicol.

border protein, carcinoembryonic antigen (CEA) (16). CEA-related cell adhesion molecules have been shown to serve as receptors for some Dr adhesins (DraE, DaaE, and AfaE-III) (16, 17).

DraE and AfaE-III are the most studied Dr adhesins. They differ in their amino acid sequences by only three residues. Recently, the crystal structure of native DraE (18) and the NMR structure of AfaE-III-Dsc were solved (19). The latter molecule contains a self-complementing β-strand that was engineered into the C terminus. The structures indicate that the assembly of Dr adhesin fimbriae is analogous to the assembly of the type 1 pilus, the P pilus, and Caf1 antigen. It has been shown that DraE and AfaE-III adhesins can form trimers if they are expressed in the absence of their chaperones (18), and the trimer structures have been solved recently, demonstrating a strand-swapped mode of assembly of the subunits (18).

The mutually interacting surfaces of the AfaE-III-DAF complex have been predicted by NMR titration experiments (19). This study revealed that the DAF binding region of AfaE-III involves a large surface comprising the A1-, A2-, B-, C2-, E-, F-, and Gd-strands (16). Previously, amino acids involved in DAF-DraE interactions had been implicated by mutagenesis studies (4).

DaaE is a fimbrial adhesin (designated F1845 in some studies) and is responsible for diffuse tissue culture cell adherence of *E. coli* C1845, a strain isolated from a child with protracted diarrhea (2). DaaE shares 57% identity with DraE at the amino acid level. In this study, we present the crystal structure of DaaE together with a mutational analysis of DaaE that together delineate the DAF-binding surface.

Homology modeling of Dr adhesins AfaE-V, AfaE-I, and NfaE-2 and binding studies of Dr adhesins DaaE, DraE, AfaE-III, AfaE-V, AfaE-I, and NfaE-2 reveal different mechanisms of DAF recognition by the members of the Dr family. We provide experimental evidence that electrostatic forces play an important role in DaaE, DraE, AfaE-III, and AfaE-V interactions with DAF and that electrostatic steering is a minor contribution to AfaE-I and NfaE-2 binding to DAF. The results of this study provide new insight into DAF-Dr adhesin associations and increase our understanding of the complex mechanisms used by pathogenic *E. coli* to cause infections.

EXPERIMENTAL PROCEDURES

Bacterial Strains—Bacterial strains were grown in Luria-Bertani (LB) or Super Broth (SB) medium at 37 °C. Clinical *E. coli* isolates from women with cystitis and pyelonephritis were kindly provided by Carl F. Marrs, University of Michigan, School of Public Health, Ann Arbor. pUC-Cm is a derivative of cloning vector pUC18 incorporating a chloramphenicol resistance cassette from pACYC184. Derivatives of pUC-Cm were grown in the presence of 25 μg/ml chloramphenicol (Cm). pCC90-D54Stop expresses the *dra* operon with a nonsense mutation in *draE* (20). Derivatives of pCC90-D54Stop, pET-21d, and pET-22b (Novagen, San Diego) were grown in 100 μg/ml ampicillin or carbenicillin. *E. coli* DH5α (Invitrogen), BL21 (DE3) (Novagen), and K12 derivative 191a (21) were hosts for the plasmids. Purification of *E. coli* chromosomal DNA, plasmid isolation, *E. coli* transformation, restriction enzyme digestion, and ligation were carried out as described (22). Enzymes were purchased from New England Biolabs (Beverly, MA) and used as recommended by the manufacturer.

Human bladder epithelial cell line T24 (ATCC HTB-4) and Chinese hamster ovary (CHO) cell transfectant clones that express human CEA or the vector alone were used (17). T24 cells were grown in McCoy's 5A medium supplemented with 10% fetal bovine serum, penicillin, and streptomycin. CHO cells were cultured in Ham's F-12 supplemented with 10% fetal bovine serum and 400 μg/ml hygromycin B. Cell lines were cultured according to standard tissue culture techniques.

Cloning, Expression, and Purification of DaaE Trimers—The mature DaaE amino acid sequence was PCR-amplified using pSSS1 (2) as a template. In preparing a construct for the purification and crystallization of DaaE, we attempted to follow the strategy of Anderson *et al.* (19) by moving the N-terminal 11 amino acids of the mature protein to the C terminus of the molecule to complete the structure formed by donor strand complementation. However, we found that removal of the N terminus had a deleterious effect on the binding properties of the purified protein (data not shown). We therefore prepared cytoplasmic proteins consisting of the entire sequence of the mature native DaaE or mutants, followed by a four amino acid linker, DNKQ, a repeat of the 11 N-terminal amino acids of the mature protein, and a C-terminal hexahistidine tag. All constructs were confirmed by sequencing using the Big Dye Terminator method and ABI sequencing (PE Applied Biosystems, Foster City, CA). The protein was expressed by pET-21d (Novagen) derivatives in *E. coli* BL21 (DE3) and purified by metal affinity chromatography followed by size exclusion chromatography on Superdex 75 (Amersham Biosciences). Although this construct provided proteins suitable for crystallization and binding studies, it did not result in self-complemented monomers.

To detect DaaE trimer-DAF complex formation, the proteins were mixed in equimolar amounts and analyzed by size exclusion chromatography on a Superdex 75 column in HBS-E buffer (10 mM HEPES (pH 7.4), 150 mM NaCl, 3 mM EDTA). The column was calibrated using gel filtration markers (Amersham Biosciences).

Cloning, Expression, and Purification of Dr Adhesins—The recombinant strains expressing DraE and AfaE-III fimbriae include strains described previously (4) and constructs described below. Cystitis-associated *E. coli* strains expressing AfaE-I and AfaE-V (23), kindly provided by Carl F. Marrs, were utilized to amplify *afaE-I* and *afaE-V*. *nfaE-2*, differing from the published sequence of its closest homolog, *nfaE-111*, by a frameshift mutation, was amplified from the diarrheal isolate SM128 (GenBank™ accession number:DQ386080). PCR products bearing the coding regions for DaaE, AfaE-I, AfaE-V, and NfaE-2 were cloned to pUC-Cm as described (4). Genes encoding Dr adhesins were amplified by using the following primers: for DraE and AfaE-III, DraE-BamHI, GGATCCGAAGGAGATATACATATGAAAAAATTAGCGATCATGGCC, and DraE-PstI, CACGCACGTCCTGCAGTCATTTTGCCCAGTAACC; for AfaE-V, DraE-BamHI primer and AfaE-V-PstI, CACGCACGCTGCAGTCAACTCACCCAGTAGCCCCAGT; for NfaE-2, NfaE-2-BamHI, CGAGGATCCGAAGGAGATATACATATGAAAATAAAATATACGATG, and NfaE-2-PstI, CACGCACGCTGCAGTTATTGGCTGTACACTGCGGC. Products were digested

with BamHI and PstI and inserted into BamHI and PstI restriction sites of pUC-Cm. The gene encoding adhesin DaaE was amplified by using the following primers: DaaE-BamHI, GGATCCGAACAGGTAATCAATATGAAAAAATTAGCGATAATG, and DaaE-EcoRI, GAATTCTTAGTTCGTCCAGTAACCCC. Product was digested with BamHI and EcoRI and inserted into BamHI and EcoRI restriction sites of pUC-Cm. The gene encoding adhesin AfaE-I was amplified by using the following primers: AfaE-I-EcoR1, GAATTCGAAGGAGATATACATATGAAAAAATTAGCGATCATAG, and AfaE-I-PstI, CACGCACGCTGCAGTTATTTTGTCCAGAACCCGCCTTCG. The product was digested with EcoRI and PstI and inserted into EcoRI and PstI restriction sites of pUC-Cm. The resulting plasmids were transformed into *E. coli* 191A (pCC90-D54Stop) or DH5α (pCC90-D54Stop). This strain contains genes of the *dra* operon necessary for fimbrial expression, with a premature stop codon at codon 54 within *draE* (no full-length DraE can be detected in this strain). All constructs were confirmed by sequencing using the Big Dye Terminator method and ABI sequencing (PE Applied Biosystems).

Dr adhesins were purified from the recombinant strains as described previously (4). For SPR analysis, adhesins were purified by gel filtration chromatography using a Superdex 200 column (Amersham Biosciences) in HBS-E buffer.

DAF234 Expression and Purification—DAF containing CCP-2, -3, and -4 with an oligohistidine tag at the C-terminal end (DAF234) was purified from recombinant *Pichia pastoris* generously provided by Dr. Susan Lea (Oxford University, Oxford, UK). DAF234 was expressed in *P. pastoris* and purified from the supernatant of induced cultures by nickel-nitrilotriacetic acid chromatography as described previously (24). For SPR experiments, the protein was then purified by gel filtration chromatography using a Superdex 200 column (Amersham Biosciences) in HBS-E buffer.

Cloning, Expression, and Purification of DAF34—PCR products with the coding regions of DAF CCP-3 and -4 (amino acids 128–251) (DAF34) were amplified using cDNA clone image ID 3460621 (ATCC) as a template and inserted into pET-22b (Novagen). The protein was expressed in *E. coli* BL21 (DE3) and purified from inclusion bodies. The inclusion bodies were dissolved overnight in buffer containing 30 mM Tris/HCl (pH 8.5), 150 mM NaCl, 1 mM EDTA, 25 mM dithiothreitol, and 8 M urea. One volume of the protein sample was added slowly to 20 volumes of the buffer containing 50 mM CHES (pH 9.2), 500 mM arginine, 1 mM reduced glutathione, and 1 mM oxidized glutathione; and the sample was left overnight at 4 °C. The refolded protein was concentrated by ultrafiltration and purified by gel filtration using a Superdex 75 column (Amersham Biosciences) in HBS-E buffer.

Surface Plasmon Resonance—SPR measurements were carried out in the running buffer: HBS-EP buffer (10 mM HEPES (pH 7.4), 150 mM NaCl, 3 mM EDTA, 0.005% P-20 surfactant (BIAcore AB, Uppsala, Sweden)) using a BIAcore 2000 system (BIAcore AB).

To analyze the interaction between DAF and DaaE trimers or DAF and Dr fimbriae, the trimers or native fimbriae were immobilized on a CM5 research-grade sensor chip (BIAcore AB) by amine coupling chemistry using the manufacturer's protocols. Immobilization of 100 response units resulted in optimal responses for Dr fimbriae-DAF, and 300 response units were immobilized for analysis of DaaE trimer-DAF interactions. DAF was dissolved in running buffer and analyzed using an $\sim 10^2$ dilution series, *i.e.* DAF (2–200 μM). Analyte was injected over the surface at a flow rate of 20 μl/min for 2 min. The affinities of the interactions were studied under steady state conditions. Average equilibrium responses were measured for six to seven concentrations of DAF. Raw sensorgrams were corrected using the double-subtraction protocol (25) and by subtracting both the reference flow cell response and the average of eight buffer injections. The resulting data were analyzed with BIAevaluation 3.0 software (BIAcore AB) to globally fit the data and derive equilibrium constants describing the intermolecular interactions. The reported K_d values are the average of at least three independent experiments. To analyze the affinity of the DaaE mutants, standard curves for binding of varying concentrations of DAF234 in solution to DaaE fimbriae or DaaE trimer immobilized on sensor chips were generated by plotting the concentration of DAF against the steady state SPR response at each concentration. For inhibition analysis and K_d calculations, varying concentrations of the mutant proteins (3–0 mg/ml) were incubated with a constant concentration of DAF234 (15 μM in running buffer) for 15–30 min. The solutions of fimbriae or trimer mutants with DAF234 were injected over DaaE fimbriae- or DaaE trimer-immobilized surfaces. Flow rate and contact time were identical to conditions used for standard curve generation. BIAevaluation software 3.0 (BIAcore) was used to calculate the K_d value by using the solution affinity model (26).

Determination of K_a and K_d Values at Different NaCl Concentrations—Binding constants were determined at different concentrations of NaCl. The running buffer included 75, 150, 300, 500, and 700 mM or 1 M NaCl. DAF for injection was prepared in each buffer so that the running buffer and DAF sample buffer were identical. The affinities of DAF for DaaE, DraE, AfaE-III, AfaE-I, AfaE-V, and NfaE-2 were determined as described above. Because the affinity of DAF for Dr adhesins decreases with increasing ionic strength, higher concentrations of DAF were used in order to bracket the K_a value for the interactions at high salt. The slope of the log K_a *versus* log [NaCl] plot was determined by linear regression.

Site-directed Mutagenesis of daaE—Mutations were introduced into the *daaE* gene on pUC-Cm or pET-21d plasmids by site-directed mutagenesis using the QuikChange® kit as directed by the manufacturer (Stratagene, La Jolla, CA). Constructs containing the mutations were identified by sequencing the *daaE* gene.

Mannose-resistant Hemagglutination Assay—Mannose-resistant hemagglutination assay with human erythrocytes of blood group O was performed as described previously (20).

Tissue Culture Cell Adherence Assay—CHO or T24 cells were split into 24-well plates with glass coverslips and grown to confluency in the tissue culture medium. Before the assay, cells were washed twice with Hanks' balanced saline solution and incubated with fresh medium without antibiotics and without fetal bovine serum for 1 h. The bacterial strains were grown

TABLE 1
Information and statistics

Crystal and unit cell information		
Crystal form	I	II
Space group	$P4_1$	P3
a	68.27 Å	72.14
b	68.27	72.14
c	97.76	77.31
α	90°	90
β	90	90
γ	90	120
No. of monomers/ asymmetric unit	3	3
Data collection statistics		
Crystal form	I	II
Molecular form	Wild type DaaE	Se-met DaaE
Beamline	ALS 5.0.1	SSRL 11-1
Resolution	1.37 Å	3.0
Measured reflections	534,397	84,621
Unique reflections	83,775	8177
Completeness (last shell)	89.4% (53.1%)	90.7% (96.1%)
R_{merge} (last shell)	0.047 (−)	0.109 (0.605)
Refinement statistics for crystal form I		
Resolution	10-1.48 Å	
R factor	0.173	
R_{free}	0.205	
No. of unique reflections	68,189	
No. of protein atoms	3516	
No. of water molecules	414	
Average *B* value, protein	19.4 $Å^2$	
Ramachandran quality	97.7% in favored regions 100.0% in allowed regions	
Root mean square deviation, bond lengths	0.010 Å	
Root mean square deviation, bond angles	1.29°	

overnight in LB medium and harvested and resuspended in 0.01 M phosphate-buffered saline (pH 7.2) to an A_{600} of 0.3. The bacterial cells were pelleted and resuspended in the tissue culture medium. Then 0.5 ml of each bacterial strain was added to each well. The adherence assay was performed as described previously (4). The experiment was repeated in triplicate.

Crystallization and Diffraction Data Collection for DaaE Adhesin—DaaE adhesin was crystallized in two crystal forms in hanging drop vapor diffusion experiments. Crystal form I (see Table 1) was obtained from a 24 mg/ml protein solution (20 mM Tris (pH 8.0), 40 mM NaCl) equilibrated against 20% PEG 4000, 0.1 M CHES buffer (pH 9.5). Crystal form II came from a 12 mg/ml protein solution (20 mM Tris (pH 8.0), 40 mM NaCl) of a selenomethionine derivative, equilibrated against 20% PEG 8000, 0.1 M CHES (pH 9.5). 30% glycerol was the cryosolvent for crystal form I, whereas crystal form II was frozen directly from the PEG 8000 solution.

The highest quality crystals were of crystal form I, tetragonal, $a = b = 68.26$ Å, $c = 97.73$ Å, space group $P4_1$. Diffraction data for the two crystal forms were collected at ALS beamline 5.0.1 and SSRL beamline 11-1. The diffraction data were processed and reduced using HKL2000 (27) as listed in Table 1. Each data set was collected using one crystal. The form II crystal showed ice rings in its diffraction pattern, and this limited the completeness of its data set.

Structure Solution and Refinement—The structures of crystal forms I and II were solved using the molecular replacement program, molrep, in the CCP-4 system (28). A subunit from the DraE structure (PDB code 1UT1 (18)) was used as the probe structure for crystal form I. Three subunits in the asymmetric unit were located by molrep using a 4 Å resolution cutoff. The three subunits made up a trimeric structure similar to those found for the related DraE and AfaE-III (18). The structure of crystal form II was obtained using a subunit from crystal form I as the probe. Again, three subunits were located in the asymmetric unit, but instead of forming a single trimer, they produce three different trimers when acted upon by the crystallographic 3-fold axes.

The structural model for crystal form I was refined using REFMAC (29) in the CCP-4 system. Statistics concerning the refinement are presented in Table 1. Anisotropic atomic displacement factors were applied for the non-hydrogen atoms. Crystal form II, because of its lower resolution, was not refined.

σA weighted $|F_o| - |F_c|$ and $2|F_o| - |F_c|$ electron density maps (30) were used to monitor and correct the refined model with XtalView (31). Residues 1–139 were located in subunit A, 1–139 in subunit B, and 1–138 in subunit C. The stereochemistry was checked during the refinement process with the programs PROCHECK (32) and MolProbity (33). The coordinates of crystal form I have been deposited in the Protein Data Bank with code 2BCM. The frames in Fig. 2 were drawn with MOLSCRIPT (34) and Raster3d (35). The surface potentials for DaaE, DraE, and DAF were calculated using the Poisson-Boltzmann equation implemented by Adaptive Poisson-Boltzmann Solver (36) and drawn with PyMOL. DraE and DAF structures used for calculations were extracted from PDB files with codes 1UT1 and1OJV.

AfaE-I, AfaE-V, and NfaE-2 Structure Prediction—Structural modeling was performed using the PROTINFO structure prediction server. Modeling was performed using the comparative modeling protocol, which has been shown to work well in the CASP protein structure prediction experiments (37, 38).

RESULTS

Crystallographic Structure Determination of DaaE—The amino acid sequence and polypeptide fold of DaaE are very similar to that of other adhesin molecules such as DraE and AfaE-III (18), see Fig. 1 for a sequence comparison. These molecules adopt an immunoglobulin-like fold (*strands A–G* in Fig. 2*A*) that forms an anti-parallel β-sandwich structure. The order and arrangement of the strands is nearly identical to those of the other closely related adhesins with the final G-strand in the β-sandwich occurring first at the N terminus of the polypeptide.

The DaaE adhesin crystallizes in two crystal forms, and the structure of each has been determined. The three DaaE monomers in the asymmetric unit of crystal form I are arranged around a noncrystallographic 3-fold rotation axis in a cyclic trimer. In crystal form II, the molecular and crystallographic 3-fold axes coincide, and the three monomers in the asymmetric unit form three crystallographically distinct trimers. Fig. 2*A* shows the structure of the trimer found in crystal form I. Refinement of the structure of crystal form II was not carried out because of the limited resolution of its diffraction pattern. The remainder of this paper will focus on the refined model for crystal form I.

Fig. 1 shows an alignment of the DraE, AfaE-III, and DaaE amino acid sequences based on an alignment of the three-dimensional structures of the proteins. The amino acid sequence identity between DaaE and DraE is 57%. There is a deletion of one residue

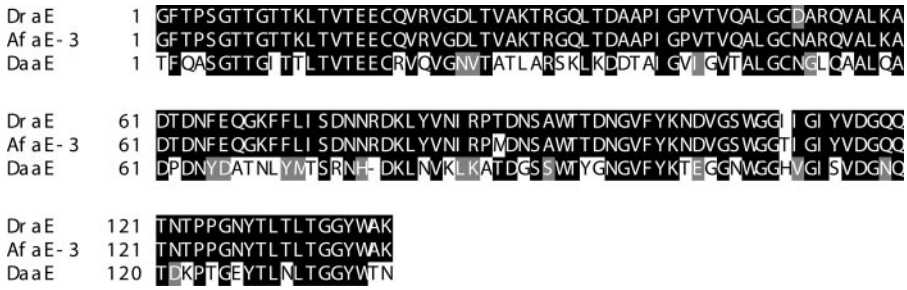

FIGURE 1. **Structure-based sequence alignments for DraE, AfaE-III, and DaaE adhesins.** Note the extra residue at position 78 in DraE and AfaE-III compared with DaaE.

in the DaaE sequence which, based on the orientations of the side chains in the structures, is best assigned to residue number 78 in the DraE sequence. The structural consequence of this is a simple adjustment of the polypeptide backbone within a few residues of the insertion site. The superposed DraE and DaaE subunits match well at residues 75 and 80 in the DraE sequence. A relatively small rearrangement of the polypeptide chain in DaaE accommodates its shorter peptide. All of this occurs in a loop away from the fundamental β-barrel structure. For the purpose of comparing the different adhesins, the residue numbers used in this report correspond to those of the DraE sequence. Accordingly, our DaaE model is missing residue number 78, even though the polypeptide chain is complete.

In all of the Dr adhesin crystal structures determined so far, the molecules assemble in the trimeric structure shown in Fig. 2*A*. In this structure, the first part of a strand (labeled A1) is extended away from the β-sandwich fold of the subunit and inserts into a neighboring subunit related by the 3-fold rotation axis. This strand insertion puts two cysteine residues (19 and 51 in DaaE) close enough together to form an inter-subunit disulfide bridge. The resulting trimers are covalently linked. However, the disulfide bridge is not essential for trimer formation. The double mutant C19S,C51S also forms trimers as shown by molecular weight measurements using gel filtration (data not shown).

To date, 16 crystallographically unique trimers have been observed in six different crystal environments for this family of proteins. Table 2 summarizes the NMR and crystal structures currently known for Dr adhesins.

The adhesin trimer, although stable, is not consistent with the DaaE fimbriae observed *in vivo*. The closed, cyclic structure does not lead to an extended fimbrial structure. In addition, the structure of the subunit in these trimers is inconsistent with evidence that an intra-subunit disulfide is found in DraE (20), not an inter-subunit disulfide. As shown in Fig. 2*A*, Cys-19 and Cys-51 within the same subunit are 45 Å apart, so some structural adjustment, including the introduction of a donor strand into the β-sandwich, would be more consistent with the physiologically important form of the adhesins.

The nature of that structural adjustment is suggested by consideration of an NMR structure determined for AfaE-III-Dsc (19). The construct used for the NMR experiments has its N-terminal donor strand relocated to its C terminus. This places it where it can act as an intra-subunit donor strand to produce monomers suitable for NMR studies. The A1- and A2-strands in the NMR structure, instead of producing a projection from the β-sandwich, form a strand within the sandwich. This rearrangement places Cys-19 and Cys-51 close enough to form an intra-subunit disulfide. Likewise, the location of the G-strand in this structure indicates where and how the donor strand binds in the fimbrial structure.

The structure of AfaE-III-Dsc provides a template for a model of the structure of DaaE in fimbriae (see Fig. 2*B*). Strands A1 and A2 become part of the β-barrel structure, although the N-terminal G-strand extends away from the subunit. This allows it to complete the β-sandwich in an adjacent subunit, forming the linked subunits characteristic of fimbriae.

The recurring trimeric structure found for the Dr adhesins is a stable conformation for these molecules when separated from the chaperone proteins involved in the natural formation of fimbriae. This has been pointed out for other members of the family (18). Prior to its inclusion in the fimbrial structure, the folded adhesin is in a semi-stable conformation that requires the presence of a β-strand from its chaperone to avoid the formation of dimers and/or other oligomers. By blocking the binding site for the projected loop seen in the trimer structure, the chaperone can thwart trimer formation and keep the A1- and A2-strands folded within the β-sandwich structure.

DaaE Mutants—DaaE binding affinity for DAF has been measured with a SPR biosensor, which enables one to detect and follow protein-protein interactions in real time. The affinities of the interactions were studied under steady state conditions by immobilizing purified DaaE fimbriae or DaaE trimers on the sensor surface and flowing soluble DAF past the adhesins. These studies indicated that the interaction between DaaE fimbriae and DAF234 was of low affinity (K_d = 17.9 ± 0.8 μM) (Table 3) with very fast on and off rates (data not shown). Despite having a different quaternary structure, DaaE trimers demonstrated the same affinity for DAF234 as do DaaE fimbriae (Table 3). As with the interaction between DAF and DaaE fimbriae, the trimer-DAF interaction was characterized by very fast on and off rates (data not shown). Moreover, when a mixture of equimolar amounts of DaaE trimer and DAF234 was analyzed by gel filtration, a peak corresponding to the DaaE trimer-DAF complex was detected, indicating the formation of a stable protein complex. No peaks corresponding to the individual proteins were detectable in significant amounts in the elution profile.

To identify DaaE amino acids involved in DAF binding, a number of mutants of DaaE were generated. These mutations were derived from our previous random mutagenesis study of DAF binding by DraE (4), and from naturally occurring variants of DraE and DaaE demonstrating altered DAF-binding phenotypes.[3] DaaE mutants were expressed as fimbriae in an isogenic

[3] N. Korotkova, S. Chattopadhyay, T. A. Tabata, V. Beskhlebnaya, V. Vigdorovich, B. K. Kaiser, R. K. Strong, D. E. Dykhuizen, E. V. Sokurenko, and S. L. Moseley, submitted for publication.

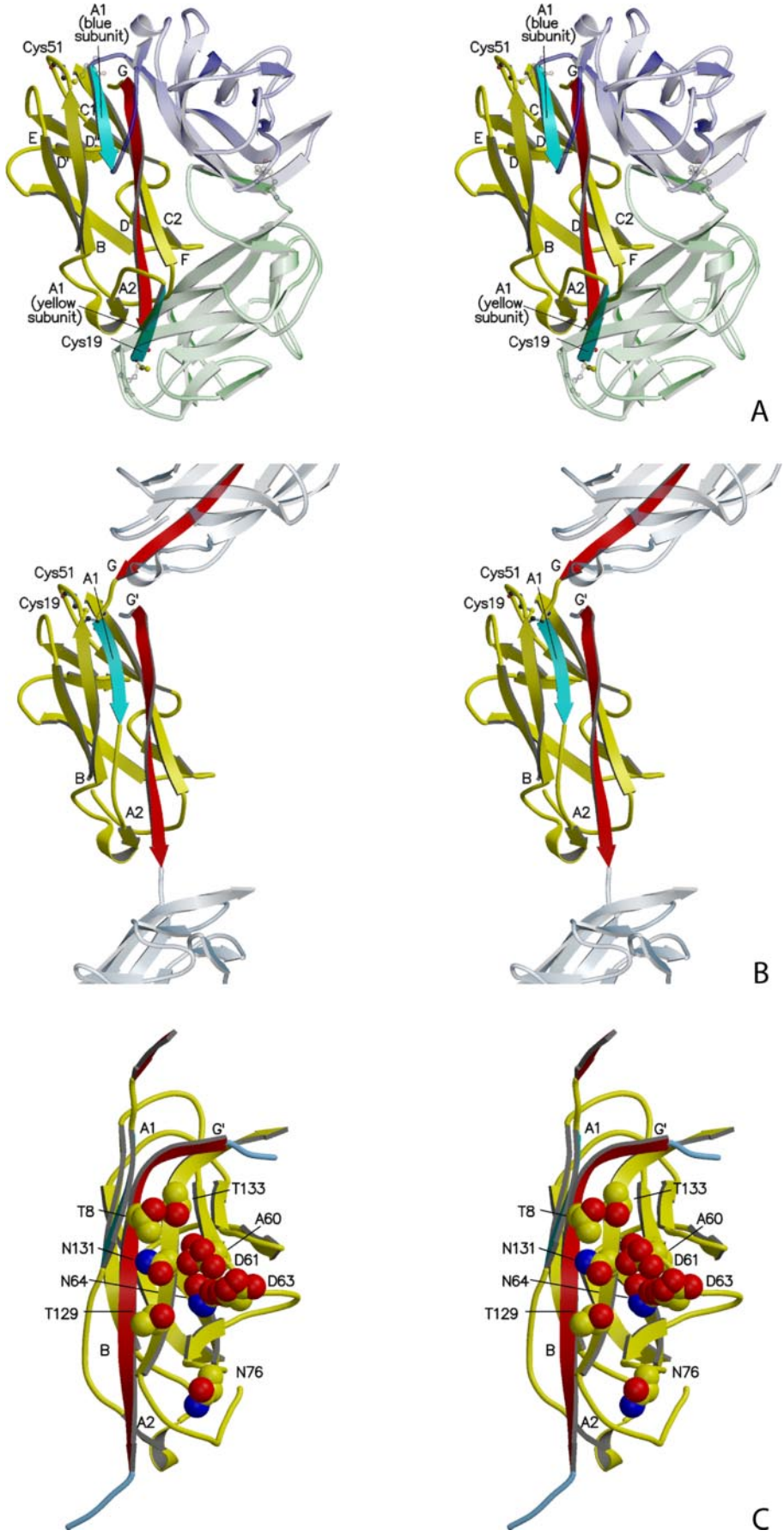

TABLE 2
Known Dr adhesin structures

PDB code	Structure	Resolution	Monomers/ asymmetric unit	crystallographically unique trimers	Ref.
		Å			
1RXL	NMR structure of AfaE-III-Dsc				19
1USQ	DraE with chloramphenicol	1.9	6	6	18
1USZ	Semet AfaE-III	3.28	1	1	18
1UT1	DraE	1.70	6	2	18
1UT2	AfaE-III	3.30	9	3	18
2BCM	DaaE (crystal form I)	1.48	3	1	This work
	DaaE (crystal form II)	3.0	3	3	This work

TABLE 3
DaaE mutants

Mutation	Source	Structure	Effect on DAF binding	MRHA	K_d ± S.E.
					μM
Wild type		Fimbriae		+	17.9 ± 0.8
T8A	Clinical	Fimbriae	Positive	+	9.1 ± 0.2
T8N	Mutagenesis	Fimbriae	Negative	−	91.1 ± 3.0
A60V	Mutagenesis	Fimbriae	Negative	−	87.2 ± 10.3
D61A	Mutagenesis	Fimbriae	Does not bind	−	
D63V	Mutagenesis	Fimbriae	Does not bind	−	
N64A	Mutagenesis	Fimbriae	Negative	+	31.6 ± 1.3
N76K	Mutagenesis	Fimbriae	Positive	+	8.5 ± 0.2
T129A	Mutagenesis	Fimbriae	Positive	+	4.2 ± 0.5
N131G	Mutagenesis	Fimbriae	Negative	−	60.9 ± 5.3
T133S	Mutagenesis	Fimbriae	Negative	−	78.4 ± 8.9
Wild type		Trimer			13.4 ± 0.4
A60V	Mutagenesis	Trimer	No effect		17.0 ± 1.3
D63V	Mutagenesis	Trimer	Does not bind		
T133S	Mutagenesis	Trimer	Negative		42.8 ± 3

E. coli background and for selected mutations as trimers. Bacteria expressing mutant fimbriae were assayed for DAF-dependent hemagglutination activity, and binding affinities of purified fimbriae and trimers for DAF234 were measured by SPR. Table 3 summarizes the DaaE mutations and their effects on DAF binding in either fimbriae or trimers. Some of the mutants enhance binding of the protein ligand, although others weaken the interactions between DaaE and DAF. The mutations at positions Asp-61 and Asp-63 have the largest effects on activity and completely abolish DAF binding. In general, shortening of the amino acid side chains tends to reduce the interaction between the proteins. Presumably, this reduces the strength of the interactions and causes a decrease in affinity (increase in K_d). However, exceptions to this pattern are noteworthy. For instance, the T8A and T129A mutants, although converting the polar side chains to the smaller methyl groups, enhance the binding affinity to DAF. On the other hand, the T8N mutant reduces the binding affinity.

The binding affinities of purified fimbriae for DAF and the observed hemagglutination phenotypes correlate in general with the ability of the variant alleles to mediate bacterial adherence to T24 human bladder epithelial cells (Fig. 3). Five mutants (T8A, A60V, D61A, D63V, and T133S) bind to a small percentage of T24 cells (2–5%) and demonstrate very low levels of binding (1–3 bacteria per T24 cell). Two mutants, T8A and T128A, with high affinity for DAF, mediate adherence of larger numbers of bacteria per T24 cell (>50) and bind to 90–100% of the epithelial cells (Fig. 3).

E. coli expressing all mutant adhesin alleles were also examined for binding to CEA, a second receptor for DaaE (16, 17). These studies were performed by observing adherence to a CHO cell line that expresses CEA. As a control, adherence to CHO cells transfected with vector alone was assessed. *E. coli* strains expressing all mutant alleles were observed to bind to 30–50% of the cells expressing CEA, whereas the parent strain lacking an adhesin gene did not bind to the cells. None of the mutant variants mediated binding of bacteria to CHO cells transfected with vector alone. These results indicate that none of the mutants result in major structural defects that adversely affect the binding competence of the fimbriae. This also suggests that DAF and CEA binding are separable phenotypes of DaaE, possibly with distinct binding domains.

Electrostatic Interactions Contribute to the Free Energy of Dr Adhesin Binding to DAF—Structural studies together with electrostatic surface analysis of DAF have revealed a

FIGURE 2. *A,* stereo view of a DaaE subunit (*colored ribbon drawing*) within the trimer found in the DaaE crystal structure. The other two subunits in the trimer are shown as *blue* and *gray* transparent ribbons. The A1-strands of the *yellow* and *blue* subunits are shown in *cyan*, and the G-strand of the *yellow* subunit is in *red.* Cysteines 19 and 51 in each subunit are shown in *ball-and-stick* representation. Strands within the *yellow* subunit are labeled. *B,* stereo view of a DaaE subunit within a model for the fimbrial structure. The G-strand for the *yellow* subunit (*red*) extends away from the molecule toward the top of the figure. The G-strand from the lower subunit, labeled *G′*, completes the β-sandwich structure for the *yellow* subunit in the donor-strand complementation process. Cysteines 19 and 51 are now located to produce an intra-subunit disulfide link. The relative locations of the subunits within the fimbria are semi-random and arbitrary. *C,* stereo view of a subunit from the fimbrial structure showing the locations of the mutations in DaaE that affect DAF affinity. Carbon atoms are drawn in *yellow.* Mutant side chains are shown in *ball-and-stick* representation with enlarged atomic radii. Alternate side chain conformers shown for Asp-61, Asp-63, and Asn-64.

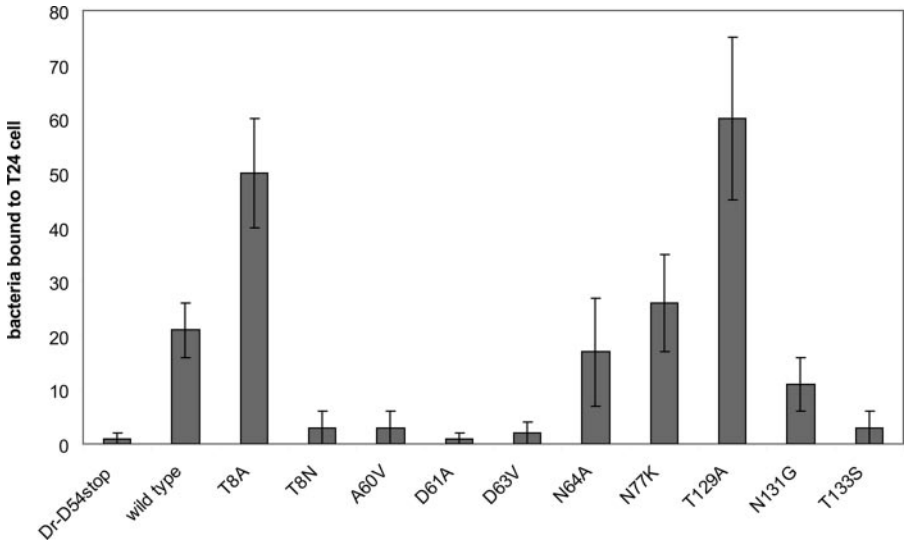

FIGURE 3. **Adherence assay of recombinant *E. coli* expressing DaaE mutant alleles.** *Black bars,* number of bacteria attaching to one T24 cell. Results shown are the average of three independent experiments. *Error bars* indicate standard deviations.

TABLE 4
Salt dependence of binding constants

Protein pair	K_d (μM) at 75 mM NaCl	K_d (μM) at 1 M NaCl
DaaE-DAF234	6.6 ± 0.4	46.7 ± 2.5
DraE-DAF234	16.0 ± 1.0	~180
AfaE-III-DAF234	8.7 ± 0.5	144 ± 11
AfaE-V-DAF234	58.9 ± 2.8	~400
AfaE-I-DAF234	9.3 ± 0.4	17.2 ± 1.1
NfaE-2-DAF234	6.6 ± 0.5	15.3 ± 0.6

positively charged cavity between the CCP-2 and CCP-3 domains of DAF, harboring three lysines (Lys-125, Lys-126, and Lys-127) (39). This flexible region is functionally critical for binding of CP and AP convertases (39–41). Our findings demonstrate that two negatively charged amino acids, Asp-61 or Asp-63, in DaaE are critical for DAF binding. Previously, it was shown that residues Asp-61, Asp-63, and Asp-75 in DraE are also important for DAF binding (4). We hypothesize that these amino acids displaying a negative surface in the adhesin can complement an electropositive region in DAF, and long range electrostatic forces together with favorable charge-charge interactions are important for adhesin-DAF complex formation. To test this hypothesis, we measured DAF234 affinity for DaaE, DraE, AfaE-III, AfaE-V, AfaE-I, and NfaE-2 adhesins at different NaCl concentrations. The buffer used for the SPR experiments contained various concentrations of NaCl ranging from 75 mM to 1 M. The binding constants for DaaE, DraE, AfaE-III, and AfaE-V with DAF234 are dependent on the concentration of NaCl, with a 7-fold decrease in binding affinity for DaaE-DAF234 interactions (see Table 4), and more than a 10-fold reduction for DraE-DAF234 and AfaE-III-DAF234. Salt also had a dramatic affect on AfaE-V-DAF234 interactions, reducing the binding affinity more than 6-fold, but the affinity at 1 M NaCl could not be estimated with confidence because it was below the sensitivity of the SPR measurements.

In contrast to the results for DaaE, DraE, AfaE-III, and AfaE-V adhesins, the binding constants for the AfaE-I-DAF234 and NfaE-2-DAF234 interactions showed less dependence on the concentration of NaCl, with only a 2-fold reduction in binding affinity between 75 mM and 1 M.

Fig. 4 shows the dependence of the association constants for DaaE, DraE, AfaE-III, AfaE-I, and NfaE-2 interactions with DAF234 on the NaCl concentration. The slope of the line, SK_{obs}, gives the net number of Na and Cl ions released or taken up by binding of the adhesin to DAF234, an indication of the contribution of electrostatic interactions to the free energy of binding (42–44). The values of SK_{obs} range from -0.68 ± 0.10 for DaaE to -1.03 ± 0.09 and -1.10 ± 0.08 for DraE and AfaE-III. However, DraE-DAF234 and AfaE-III-DAF234 interactions are more electrostatically steered than is the DaaE-DAF234 interaction. The strength of this interaction is comparable with the electrostatic interaction between thrombin and the highly charged C-terminal tail of its inhibitor hirudin (which forms three salt bridges at the interface) ($SK_{obs} = -1.1$) (42, 45).

To determine the contribution of electrostatic interactions to the overall free energy of binding, we compared the ΔG values at 75 mM NaCl with those at 1 M NaCl, conditions assumed to eliminate electrostatic interactions. Electrostatic steering contributes less than 7% to the overall free energy of binding in the AfaE-I-DAF and NfaE-2-DAF interactions, ~16% in the DaaE-DAF234 interactions, and more than 40% in the AfaE-III-DAF234 and DraE-DAF234 interactions. Taken together, these results demonstrate that Dr adhesins use different mechanisms to interact with DAF.

Binding of Dr Adhesins to DAF234 and DAF34—We utilized SPR to investigate DAF34 binding to Dr adhesins DaaE, DraE, AfaE-III, AfaE-V, AfaE-I, and NfaE-2. DAF34 did not show detectable binding to DaaE, DraE, AfaE-III, and AfaE-V adhesins, all of which show significant electrostatic interactions with DAF234. In contrast, DAF34 did bind AfaE-I and NfaE-2 ($K_d = 17.1 \pm 0.8$ μM for AfaE-I and $K_d = 13.6 \pm 0.5$ μM for NfaE-2). Because electrostatic forces do not contribute significantly to AfaE-I and NfaE-2 interactions with DAF234 (Fig. 4), and these adhesins do not require CCP-2 for binding to DAF, these observations suggest that CCP-2 or the positively charged linker region between CCP-2 and -3 contribute to the electrostatic interactions between DAF and DaaE, DraE, AfaE-III, and AfaE-V.

Predicted Structure Analysis of AfaE-I, AfaE-V, and NfaE-2 Adhesins—To better understand the nature of Dr adhesin interactions with DAF, three-dimensional structures were modeled for AfaE-I, AfaE-V, and NfaE-2 based on the experimentally determined structures of DraE (PDB 1UT1) and DaaE (this study). The highest probability models of AfaE-I, AfaE-V, and NfaE-2, as well as the DraE and DaaE structural models were utilized to calculate surface potentials (Fig. 5). We found

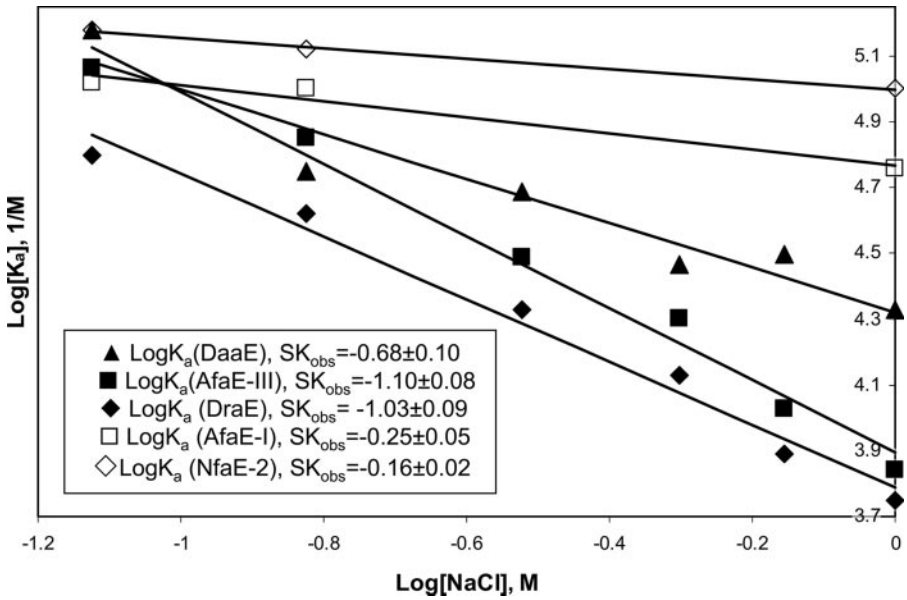

FIGURE 4. **Analysis of salt dependence of binding.** K_a values of DaaE/DAF, AfaE-III/DAF, AfaE-I/DAF, NfaE-2/DAF, and DraE/DAF were determined as a function of NaCl concentration from SPR experiments. The data were fit by linear regression to determine the values of SK_{obs} for each set of binding partners.

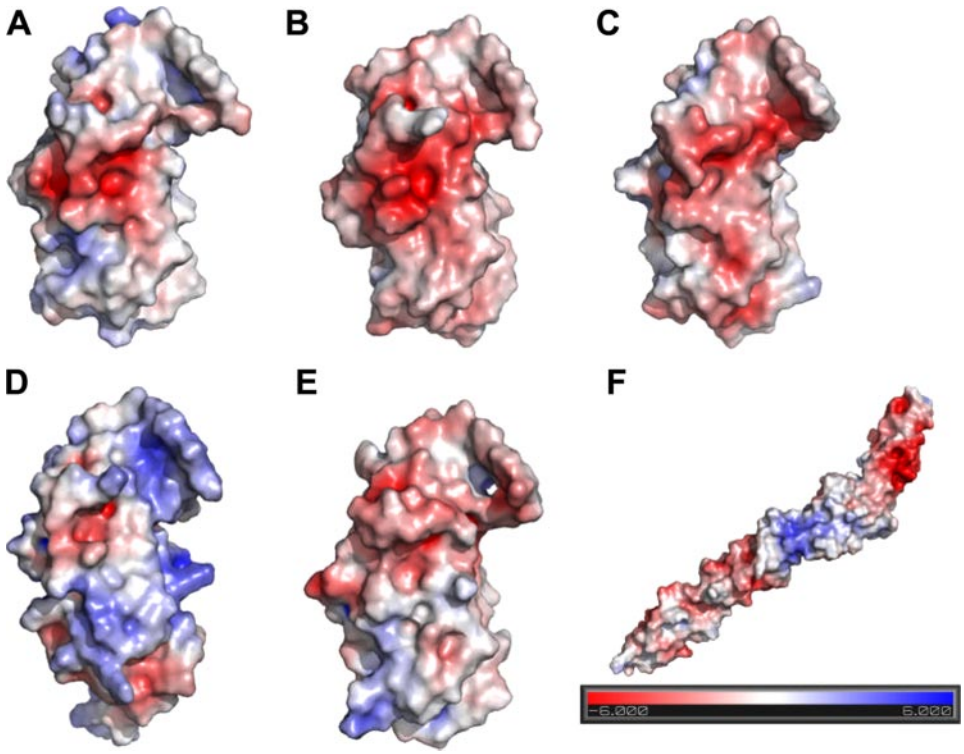

FIGURE 5. **Surface electrostatic potentials of DraE (*A*), DaaE (*B*), AfaE-V (*C*), AfaE-I (*D*), NfaE-2 (*E*), and DAF (*F*).** The surface potentials for Dr adhesins and DAF were calculated using the Poisson-Boltzmann equation implemented by Adaptive Poisson-Boltzmann Solver and drawn with PyMOL. DraE and DAF structures used for calculations were extracted from PDB files with codes 1UT1 and 1OJV. Predicted structures of AfaE-V, AfaE-I, and NfaE-2 were created by RAMP software. *Red* denotes negative charge and *blue* denotes positive charge.

that the local charge distributions differ for DraE, DaaE, AfaE-I, AfaE-V, and NfaE-2. DraE, DaaE, and AfaE-V display a clustering of negatively charged surfaces located within the DAF binding region identified by mutagenesis and described above. AfaE-I and NfaE-2 do not show a similar clustering of negative charge, consistent with our observations that electrostatic interactions do not contribute significantly to DAF binding by these adhesins.

DISCUSSION

In our previous studies of DraE-DAF interactions, we utilized a mutagenesis approach together with homology modeling to identify the amino acids of DraE involved in binding. In this study we have used structural and functional analyses of DaaE to further investigate DAF recognition by Dr adhesins.

DaaE mutations affecting DAF binding can be mapped onto the fimbrial model of DaaE (see Fig. 2*C*). This cluster of residues is in an area consistent with previous genetic analysis of DraE binding to DAF (4), the crystal structure of DraE trimers (18), and the DAF-binding site proposed from NMR studies of AfaE-III-Dsc (19). Nine of the mutation sites are clustered on the surface of the adhesin (residues 8, 60, 61, 63, 64, 76, 129, 131, and 133). Seven of them (8, 61, 63, 76, 129, 131, and 133) are solvent-accessible and are shown in Fig. 2*C*. The 8th residue listed in Table 3, A60V, maps to a site where the side chains point toward the center of the protein (Fig. 2*D*). This interior mutant is located near the cluster of surface residues in the DAF-binding site. It seems likely that the mutation might influence the overall stability of that cluster and thus affect the affinity for DAF.

The 9th residue in this cluster is Asn-64. Its side chain is directed toward the molecular surface from the β-barrel, but it is buried by the other residues in this cluster (see Fig. 2*C*). In particular, the side chain of this residue is in close contact with those of residues 61 and 63. The orientations of the side chains of this set of residues are consistent with a role for them in constituting a binding surface for DAF. Changes in the sizes and polarities of the residues could account for the effects of their mutations on the K_d value for binding of DAF. Our binding studies demonstrate that the mutations introduced at positions Asp-61 and Asp-63 of DaaE have the greatest effects on activity, completely abolishing DAF binding. Previous functional analyses of DraE support the idea that the negatively charged amino

acids Asp-61, Asp-63, and Asp-75 are important for DAF binding (4).

As expected, calculation of the electrostatic potentials for the DraE and DaaE structures revealed an electronegative region around the cluster of residues involved in DAF recognition (Asp-61, Asp-63, and Glu-126 of DaaE and Asp-61, Asp-63, and Asp-75 of DraE) (Fig. 5). Similar electrostatic properties shared by a set of proteins may indicate similar behavior and function (46), so the electrostatic potentials of the Dr adhesins, including AfaE-I, AfaE-V, and NfaE-2, were compared using the DaaE and DraE structures (PDB code 1UT1) as examples.

From inspection of Fig. 5, it is evident that AfaE-V, NfaE-2, and AfaE-I adhesins also have negative amino acids located within the region described above. The AfaE-I and NfaE-2 structural models do not reveal a similar clustering of negative charge, suggesting that these adhesins use a mechanism for DAF recognition that differs from that of DraE, DaaE, and AfaE-V. It is known that high concentrations of NaCl reduce long range electrostatic interactions and limit salt bridge formation. Thermodynamic analysis of adhesin-DAF interactions at various salt concentrations revealed that DraE-DAF and AfaE-III-DAF interactions are highly dependent on ionic strength, and electrostatic forces contribute more than 40% to their free energy of binding. Salt had less effect on DaaE-DAF interactions. Although Asp-61 and Asp-63 in DaaE contribute to ion pairing, the DaaE-DAF recognition is more dependent on other binding forces such as hydrogen bonds and hydrophobic contacts. Salt dramatically reduces the AfaE-V-DAF binding affinity and makes it impossible to observe the AfaE-V-DAF complex using SPR.

The minor effect of salt on AfaE-I-DAF and NfaE-DAF interactions stands in sharp contrast to its effect on the DraE-DAF complex. DAF binding to AfaE-I and NfaE-2 involves mostly hydrophobic forces and hydrogen bonds. This observation is consistent with analysis of the electrostatic surfaces of AfaE-I and NfaE-2. Therefore, despite possessing similar structures, members of the Dr adhesins family use different mechanisms to bind DAF.

Dr adhesins display negatively charged surfaces that could complement an electropositive region in DAF (Fig. 5*A*). Uhrinova *et al.* (39) have pointed out an area of positive charge located near the CCP-2,3 interface in the DAF structure (Fig. 5*C*). Our binding analysis of DAF34 with Dr adhesins reveals that this electropositive region with CCP-2 is required only for interactions with DraE, AfaE-III, DaaE, and AfaE-V, *i.e.* those adhesins showing significant electrostatic interactions with DAF. Taken together, our data show that the recognition areas of DAF are not identical for all Dr adhesins.

The positively charged cavity between the CCP-2 and CCP-3 domains of DAF is important for AP and CP regulatory activities and likely contacts the convertases of the complement cascade (39, 40). Thus, DAF interactions with Dr adhesins might inhibit complement regulation, leading to increased susceptibility of the target epithelial cell to complement-mediated damage, or possibly protection of bound *E. coli* against complement attack. Indeed, Anderson *et al.* (19) observed that binding AfaE-III to DAF antagonized DAF regulation of the AP convertase C3bBb.

It has been found that this functionally critical region of DAF is semiflexible and involved in loose hydrophobic contact with side chains of CCP-2 and CCP-3 (39). This functional property of DAF could be a requirement for the ability of DAF to interact with the convertases and accelerate their decay (39). It is not yet clear whether DAF undergoes a conformational transition after binding to the convertases. However, recognition of DAF by the Dr adhesin triggers complex signal transduction cascades leading to internalization of *E. coli* (47, 48). The emerging picture of DAF-adhesin interactions is consistent with DAF binding to an electropositive region of DAF that results in perturbation of the interactions between CCP-2 and CCP-3. The conformational transition of DAF after the adhesin attachment could transmit an allosteric signal to the intracellular milieu, triggering cellular responses that result in clustering of DAF around bacterial cells and recruitment of the other surface structures such as CEA-related cell adhesion molecule receptors, and $\alpha_{5\beta1}$ integrin for the uptake of *E. coli*.

Extensive mutagenesis data and binding studies reveal that ionic interactions form an essential component of the binding interface between CCPs (DAF, factor H, CR1, C4BP, and MCP) and C3b/C4b (49–52). Such functional similarity of several complement regulators is because of the presence of negatively charged amino acids on the surface of C4b and C3b that are complemented by positively charged patches present on the molecular surface of complement-control proteins (53). Many pathogens, including *Streptococcus pyogenes, Bordetella pertussis, Neisseria* sp., *Moraxella catarrhalis, Treponema denticola,* and *Borrelia* sp. bind to these negatively charged sites within complement inhibitors (54). Attachment to an evolutionarily conserved site in a complement inhibitor, rather than a region that is susceptible to change, might be favorable for pathogens. Moreover, binding to complement-control proteins might result in local down-regulation of the host complement system, thereby increasing the pathogenicity of these bacteria.

Our model predicts that Dr adhesins such as AfaE-I and NfaE that do not require interaction with the positively charged region between domains CCP-2 and CCP-3 may differ from the other Dr adhesins in their signaling capacity. Our study thus provides a basis for the design of further experiments with this system.

Acknowledgments—We are grateful to Evgeni V. Sokurenko and Veronika L. Chesnokova for helpful criticism of the manuscript, Tami Tabata and Diane Capps for technical assistance, and Jürgen Bosch and Mark Robien for helpful discussions. We thank Alain L. Servin (INSERM) for kindly providing CHO cells that express CEA and pCEAP4 and David J. Evans (Institute of Virology, University of Glasgow) for generously providing the constructs for DAF234 expression. The diffraction data sets used in this study were obtained at the Advanced Light Source and the Stanford Synchrotron Radiation Laboratory. The Advanced Light Source is supported by the Director, Office of Science, Office of Basic Energy Sciences, of United States Department of Energy under Contract DE-AC02-05CH11231. The SSRL Structural Molecular Biology Program is supported by the Department of Energy, Office of Biological and Environmental Research, and by the National Institutes of Health, National Center for Research Resources, Biomedical Technology Program, and the National Institute of General Medical Sciences.

REFERENCES

1. Servin, A. L. (2005) *Clin. Microbiol. Rev.* **18,** 264–292
2. Bilge, S. S., Clausen, C. R., Lau, W., and Moseley, S. L. (1989) *J. Bacteriol.* **171,** 4281–4289
3. Swanson, T. N., Bilge, S. S., Nowicki, B., and Moseley, S. L. (1991) *Infect. Immun.* **59,** 261–268
4. Van Loy, C. P., Sokurenko, E. V., Samudrala, R., and Moseley, S. L. (2002) *Mol. Microbiol.* **45,** 439–452
5. Le Bouguenec, C., Garcia, M. I., Ouin, V., Desperrier, J. M., Gounon, P., and Labigne, A. (1993) *Infect. Immun.* **61,** 5106–5114
6. Labigne-Roussel, A. F., Lark, D., Schoolnik, G., and Falkow, S. (1984) *Infect. Immun.* **46,** 251–259
7. Sauer, F. G., Remaut, H., Hultgren, S. J., and Waksman, G. (2004) *Biochim. Biophys. Acta* **1694,** 259–267
8. Zavialov, A. V., Berglund, J., Pudney, A. F., Fooks, L. J., Ibrahim, T. M., MacIntyre, S., and Knight, S. D. (2003) *Cell* **113,** 587–596
9. Choudhury, D., Thompson, A., Stojanoff, V., Langermann, S., Pinkner, J., Hultgren, S. J., and Knight, S. D. (1999) *Science* **285,** 1061–1066
10. Sauer, F. G., Futter, K., Pinkner, J. S., Dobson, K. W., Hultgren, S. J., and Waksman, G. (1999) *Science* **285,** 1058–1061
11. Nicholson-Weller, A., and Wang, C. E. (1994) *J. Lab. Clin. Med.* **123,** 485–491
12. Medof, M. E., Walter, E. I., Rutgers, J. L., Knowles, D. M., and Nussenzweig, V. (1987) *J. Exp. Med.* **165,** 848–864
13. Brodbeck, W. G., Liu, D., Sperry, J., Mold, C., and Medof, M. E. (1996) *J. Immunol.* **156,** 2528–2534
14. Hasan, R. J., Pawelczyk, E., Urvil, P. T., Venkatarajan, M. S., Goluszko, P., Kur, J., Selvarangan, R., Nowicki, S., Braun, W. A., and Nowicki, B. J. (2002) *Infect. Immun.* **70,** 4485–4493
15. Nowicki, B., Hart, A., Coyne, K. E., Lublin, D. M., and Nowicki, S. (1993) *J. Exp. Med.* **178,** 2115–2121
16. Guignot, J., Peiffer, I., Bernet-Camard, M. F., Lublin, D. M., Carnoy, C., Moseley, S. L., and Servin, A. L. (2000) *Infect. Immun.* **68,** 3554–3563
17. Berger, C. N., Billker, O., Meyer, T. F., Servin, A. L., and Kansau, I. (2004) *Mol. Microbiol.* **52,** 963–983
18. Pettigrew, D., Anderson, K. L., Billington, J., Cota, E., Simpson, P., Urvil, P., Raduzin, F., Roversi, P., Nowicki, B., du Merle, L., Le Bouguénec, C., Matthews, S., and Lea, S. M. (2004) *J. Biol. Chem.* **279,** 46851–46857
19. Anderson, K. L., Billington, J., Pettigrew, D., Cota, E., Simpson, P., Roversi, P., Chen, H. O., Urvil, P., du Merle, L., Barlow, P. N., Medof, M. E., Smith, R. A. G., Nowicki, B., Le Bouguénec, C., Lea, S. M., and Matthews, S. (2004) *Mol. Cell* **15,** 647–657
20. Carnoy, C., and Moseley, S. L. (1997) *Mol. Microbiol.* **23,** 365–379
21. Klemm, P., Jorgensen, B. J., van Die, I., de Ree, H., and Bergmans, H. (1985) *Mol. Gen. Genet.* **199,** 410–414
22. Maniatis, T., Fritsch, E. F., and Sambrook, J. (1982) *Molecular Cloning: A Laboratory Manual*, pp. 98–148; 249–253, Cold Spring Harbor Laboratory Press, Cold Spring Harbor, NY
23. Zhang, L., Foxman, B., Tallman, P., Cladera, E., Le Bouguénec, C., and Marrs, C. F. (1997) *Infect. Immun.* **65,** 2011–2018
24. Powell, R. M., Ward, T., Evans, D. J., and Almond, J. W. (1997) *J. Virol.* **71,** 9306–9312
25. Myszka, D. G. (1999) *J. Mol. Recognit.* **12,** 279–284
26. Adamczyk, M. J., Moore, A., and Yu, Z. (2000) *Methods* (*Orlando*) **20,** 319–328
27. Otwinowski, Z., and Minor, W. (1997) *Methods Enzymol.* **276,** 307–326
28. Collaborative Computational Project (1994) *Acta Crystallogr. Sect. D Biol. Crystallogr.* **50,** 760–763
29. Murshudov, G. N., Vagin, A. A., and Dodson, E. J. (1997) *Acta Crystallogr. Sect. D Biol. Crystallogr.* **53,** 240–255
30. Read, R. J. (1986) *Acta Crystallogr. Sect. A* **42,** 140–149
31. McRee, D. E. (1999) *J. Struct. Biol.* **125,** 156–165
32. Laskowski, R. A., MacArthur, M. W., Moss, D. S., and Thornton, J. M. (1993) *J. Appl. Crystallogr.* **26,** 283–291
33. Lovell, S. C., Davis, I. W., Arendall, S. B. I., de Bakker, P. I. W., Word, J. M., Prisant, M. G., Richardson, J. S., and Richardson, D. C. (2003) *Proteins Struct. Funct. Genet.* **50,** 437–450
34. Kraulis, P. J. (1991) *J. Appl. Crystallogr.* **24,** 946–950
35. Merritt, E. A., and Bacon, D. J. (1997) *Methods Enzymol.* **277,** 505–524
36. Baker, N. A., Sept, D., Joseph, S., Holst, M. J., and McCammon, J. A. (2001) *Proc. Natl. Acad. Sci. U. S. A.* **98,** 10037–10041
37. Hung, L.-H., and Samudrala, R. (2003) *Nucleic Acids Res.* **31,** 3296–3299
38. Hung, L.-H., Ngan, S.-C., Liu, T., and Samudrala, R. (2005) *Nucleic Acids Res.* **33,** W77–W80
39. Uhrinova, S., Lin, F., Ball, G., Bromek, K., Uhrin, D., and Medof, M. E. (2003) *Proc. Natl. Acad. Sci. U. S. A.* **100,** 4718–4723
40. Brodbeck, W. G., Kutner-Kondo, L., Mold, C., and Medof, M. E. (2000) *Immunology* **101,** 104–111
41. Kuttner-Kondo, L. A., Mitchell, L., Hourcade, D. E., and Medof, M. E. (2001) *J. Immunol.* **167,** 2164–2171
42. Grucza, R. A., Bradshaw, J. M., Mitaxov, V., and Waksman, G. (2000) *Biochemistry* **39,** 10072–10081
43. Record, M. T., and Anderson, C. F. (1995) *Biophys. J.* **68,** 786–794
44. Herr, A. B., White, C. L., Milburn, C., Wu, C., and Bjorkman, P. J. (2003) *J. Mol. Biol.* **327,** 645–657
45. de Cristofaro, R., Fenton, J. W. I., and Di Cera, E. (1992) *J. Mol. Biol.* **226,** 263–269
46. Soares, D. C., Gerloff, D. L., Syme, N. R., Colson, A. F., Parkinson, J., and Barlow, P. N. (2005) *Protein Eng. Des. Sel.* **18,** 379–388
47. Selvarangan, R., Goluszko, P., Singhal, J., Carnoy, C., Moseley, S., Hudson, B., Nowicki, S., and Nowicki, B. (2004) *Infect. Immun.* **72,** 4827–4835
48. Kansau, I., Berger, C., Hospital, M., Amsellem, R., Nicolas, V., Servin, A. L., and Bernet-Camard, M. F. (2004) *Infect. Immun.* **72,**
49. Blom, A. M., Zadura, A. F., Villoutreix, B. O., and Dahlback, B. (2000) *Mol. Immunol.* **37,** 445–453
50. Blom, A. M., Kask, L., and Dahlback, B. (2003) *Mol. Immunol.* **39,** 547–556
51. Giannakis, E., Jokiranta, T. S., Male, D. A., Ranganathan, S., Ormsby, R. J., Fischetti, V. A., Mold, C., and Gordon, D. L. (2003) *Eur. J. Immunol.* **33,** 963–969
52. Morikis, D., and Lambris, J. D. (2004) *J. Immunol.* **172,** 7537–7547
53. Oran, A. E., and Isenman, D. E. (1999) *J. Biol. Chem.* **274,** 5120–5130
54. Lindahl, G., Sjobring, U., and Jonnsson, E. (2002) *Curr. Opin. Immunol.* **12,** 44–51